



Behavior of quasinormal modes and high dimension RN-AdS black hole phase transition

M. Chabab^{1,a}, H. El Moumni^{1,2,b}, S. Iraoui^{1,c}, K. Masmar^{1,d}

¹ High Energy Physics and Astrophysics Laboratory, Faculty of Science Semlalia, Cadi Ayyad University, 40000 Marrakesh, Morocco

² LMTI, Physics Department, Faculty of Sciences, Ibn Zohr University, Agadir, Morocco

Received: 17 September 2016 / Accepted: 14 November 2016 / Published online: 7 December 2016

© The Author(s) 2016. This article is published with open access at Springerlink.com

Abstract In this work we use the quasinormal frequencies of a massless scalar perturbation to probe the phase transition of the high dimension charged AdS black hole. The signature of the critical behavior of this black hole solution is detected in the isobaric as well as in isothermal process. This paper is a natural generalization of Liu et al. (JHEP 1409:179, 2014) to higher dimensional spacetime. More precisely our study shows a clear signal for any dimension d in the isobaric process. As to the isothermal case, we find that this signature can be affected by other parameters like the pressure and the horizon radius. We conclude that the quasinormal modes can be an efficient tool to investigate the first-order phase transition, but fail to disclose the signature of the second-order phase transition.

1 Introduction

Since the original work of Vishveswara [2, 3] on quasinormal modes (QNMs), considered as solutions of a perturbed wave equation around black hole configuration, interest has been increasing in their study. Indeed the characteristic oscillations of the black holes play a prominent role in the dynamics of astrophysical black holes in the framework of general relativity [4, 5]. Last February, LIGO (Laser Interferometer Gravitational-Wave Observatory) announced for the first time the detection of gravitational waves from a cosmic event generated more than one billion year ago by the merger of two orbiting black holes [6]. The observation of these waves is an important landmark in the gravitational waves astronomy. The measure of the QNMs frequencies by various detectors such as LIGO [7], VIRGO [8], KAGRA [9, 10], can shed

light on the main feature of the black holes such the mass and the angular momentum.

The properties of quasinormal modes have been tested in the context of the AdS/CFT correspondence [11–13], the investigation of the stability of AdS black holes becomes more appealing. The quasinormal frequencies of AdS black holes have direct interpretation in terms of the dual conformal field theory CFT, for details we refer to [14–20]. The QNMs can be used as a powerful tool to detect the extra dimensions of spacetime, in other words the brane-world scenarios assume the existence of extra dimensions, so that multidimensional black holes can be formed in a laboratory [21–24].

Recently, many efforts have been devoted to the study of the thermodynamical properties of black holes, in connection with higher dimensional supergravity models [25, 26]. These properties have been extensively studied via different methods including numerical computation using various codes [27]. In fact, several models based on mathematical methods have been explored to study critical behaviors of black holes with different geometrical configurations in arbitrary dimensions. A particular emphasis has been put on AdS black holes [28–34]. More precisely, a nice interplay between the behaviors of the RN-AdS black hole systems and the Van der Waals fluids has been discussed at length in [35–43].

In this context, several landmarks of statistical liquid-gas systems, such as the P - V criticality, the Gibbs free energy, the first-order phase transition and the behavior near the critical points have been derived. Also, in [1] the authors established a link between the Reissner-Nordström AdS black hole critical behavior and the quasinormal modes in $d = 4$, showing that QNM can be a dynamic probe of the thermodynamic phase transition. More precisely they find a drastic change in the slopes of the quasinormal frequencies in the small (SBH) and large (LBH) black holes near the critical point where the Van der Waals like thermodynamic phase transition occurs. Also in [44], the authors studied the quasinormal modes and

^a e-mail: mchabab@uca.ac.ma

^b e-mail: hasan.elmoumni@edu.uca.ma

^c e-mail: s.iraoi@edu.uca.ma

^d e-mail: karima.masmar@edu.uca.ac.ma

P - V criticality for scalar perturbations in a class of dRGT massive gravity around Black Holes.

Motivated by these results we find it crucial and well justified to generalize these studies to high dimensional spacetime, since a higher dimension RN–AdS black hole also presents a Van der Waals like phase transition [35, 37].

Our paper is organized as follows. We briefly review the critical behavior of the charged-AdS black hole in arbitrary dimensional spacetime in Sect. 2. In Sect. 3 we develop the master equation for the massless scalar field perturbation in high dimensional RN–AdS spacetime. Sections 4 and 5 are devoted to the calculation of the quasinormal modes of scalar perturbation around the black holes and to show how their frequencies encode the signature of the first-order phase transition. Also we will see that the QNMs cannot reveal the second-order phase transition. In Sect. 6 we discuss how the critical ratio affects the ability of the quasinormal modes frequencies to detect the phase transition. Finally, in the last section we summarize our results and draw the conclusion.

2 Critical behavior of RN–AdS black holes in higher dimension: a review

The Einstein–Maxwell–Anti-de Sitter action in higher dimensions d may be written as

$$I_{\text{EM}} = -\frac{1}{16\pi} \int_M d^d x \sqrt{-g} \left(R - F^2 + \frac{(d-1)(d-2)}{l^2} \right). \quad (1)$$

The solution of the action (1) is the solution for a spherical d -dimensional charged AdS black hole with negative cosmological constant where $d \geq 4$. It can be written in the static form

$$\begin{aligned} ds^2 &= -f dt^2 + \frac{dr^2}{f} + r^2 d\omega_{d-2}^2, \\ F &= dA, \quad A = -\sqrt{\frac{d-2}{2(d-3)}} \frac{q}{r^{d-3}} dt. \end{aligned} \quad (2)$$

Here, the function f is given by

$$f = 1 - \frac{m}{r^{d-3}} + \frac{q^2}{r^{2(d-3)}} + \frac{r^2}{l^2}, \quad (3)$$

and $d\omega_d^2$ is the metric of a d -dimensional unit sphere.

The parameters m and q are related to the ADM mass M (in our set up, they are associated with the enthalpy of the system as we shall see later) and the charge Q of the black hole by [31]

$$\begin{aligned} M &= \frac{d-2}{16\pi} \omega_{d-2} m, \\ Q &= \frac{\sqrt{2(d-2)(d-3)}}{8\pi} \omega_{d-2} q, \end{aligned} \quad (4)$$

with ω_d being the volume of the unit d -sphere,

$$\omega_d = \frac{2\pi^{\frac{d+1}{2}}}{\Gamma(\frac{d+1}{2})}. \quad (5)$$

It is worth to notice that the cosmological constant $\Lambda = -\frac{(d-1)(d-2)}{2l^2}$ is regarded as a variable and also identified with the thermodynamic pressure P [45–47],

$$P = -\frac{1}{8\pi} \Lambda = \frac{(d-1)(d-2)}{16\pi l^2}, \quad (6)$$

in the geometric units $G_d = \hbar = c = k_B = 1$. The corresponding conjugate quantity, namely the thermodynamic volume, is given by [33]

$$V = \frac{\omega_{d-2} r_H^{d-1}}{d-1}, \quad (7)$$

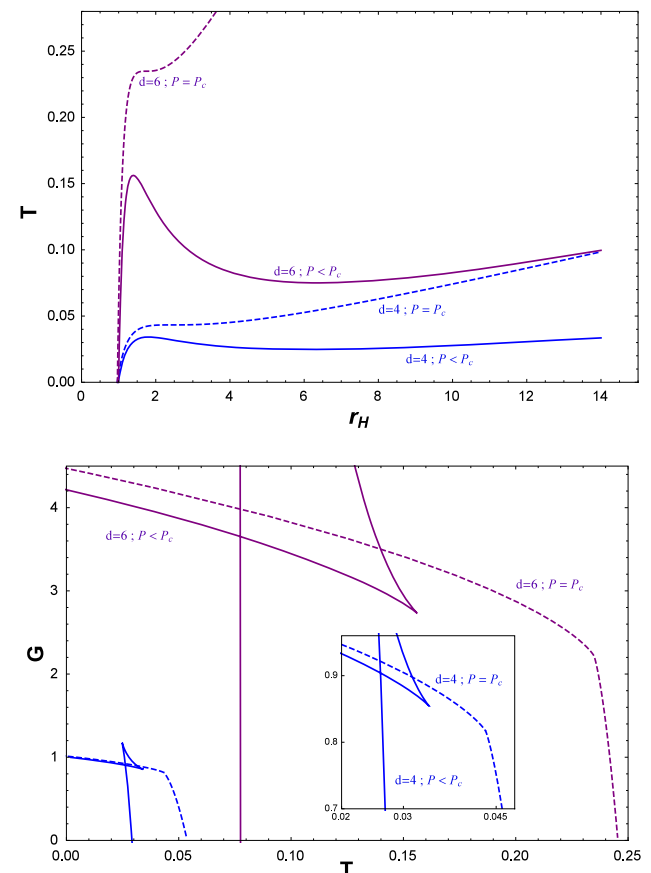


Fig. 1 Top the Hawking temperature as a function of the black holes horizon r_H in $d = 4, 6$. Bottom the Gibbs free energy as a function of the temperature T in $d = 4, 6$. The two upper lines (purple) correspond to $d = 6$ while the lower one (blue) correspond to $d = 4$. The critical isobar $P = P_c$ is denoted by the dashed lines, while the solid lines show the first-order transition $P < P_c$

Table 1 The quasinormal frequencies of the massless scalar perturbation as a function of the black holes temperature. The upper part, above the horizontal lines is for the small black hole phase while the lower part is for the large one

T	r_H	ω_r	ω_{im}	T	r_H	ω_r	ω_{im}
$d = 4; P = 0.000331573$, and $T_c = 0.0158676$				$d = 5; P = 0.00205468$ and $T_c = 0.0439405$			
0.013	1.09711	0.140236	-0.00361077	0.036	1.06452	0.35998	-0.00328399
0.0135	1.10221	0.140229	-0.00361519	0.037	1.06699	0.359975	-0.00328714
0.014	1.10743	0.140222	-0.00361991	0.038	1.0695	0.35997	-0.00329046
0.0145	1.11279	0.140214	-0.00362496	0.04	1.07464	0.35996	-0.00329765
0.015	1.11829	0.140206	-0.00363038	0.041	1.07729	0.359954	-0.00330155
0.0155	1.12395	0.140197	-0.0036362	0.043	1.08273	0.359942	-0.00331004
0.016	17.1569	0.141771	-0.127259	0.044	10.5599	0.420898	-0.231517
0.0165	18.3675	0.145464	-0.136319	0.045	11.2726	0.433701	-0.249332
0.017	19.4967	0.149092	-0.144749	0.046	11.9157	0.445686	-0.265327
0.0175	20.5692	0.152686	-0.152739	0.047	12.5136	0.457162	-0.280141
0.018	21.5996	0.156262	-0.160405	0.048	13.0794	0.46829	-0.294112
0.0185	22.5974	0.159829	-0.167819	0.049	13.621	0.479167	-0.307447
$d = 6; P = 0.0058964$ and $T_c = 0.0773752$				$d = 7; P = 0.0122899$ and $T_c = 0.114151$			
0.074	1.06156	0.60234	-0.00223733	0.106	1.04847	0.85745	-0.00138892
0.0745	1.06216	0.602339	-0.00223825	0.107	1.04913	0.857449	-0.00138971
0.075	1.06277	0.602338	-0.00223919	0.11	1.05116	0.857446	-0.00139219
0.0755	1.06338	0.602337	-0.00224014	0.112	1.05254	0.857444	-0.00139395
0.076	1.06399	0.602336	-0.00224111	0.113	1.05324	0.857443	-0.00139486
0.077	1.06523	0.602333	-0.00224309	0.114	1.05394	0.857442	-0.0013958
0.0775	8.21528	0.731459	-0.28622	0.115	7.20019	1.05914	-0.32404
0.078	8.41977	0.739944	-0.295132	0.116	7.4564	1.07735	-0.339388
0.0785	8.61178	0.748027	-0.30348	0.117	7.69002	1.09429	-0.353327
0.079	8.79399	0.755798	-0.311384	0.118	7.90753	1.11033	-0.366262
0.0795	8.96824	0.763316	-0.318927	0.119	8.11287	1.12569	-0.378435
0.08	9.13587	0.770627	-0.326169	0.12	8.30858	1.14053	-0.390003
$d = 8; P = 0.021516$ and $T_c = 0.153223$				$d = 9; P = 0.0337696$ and $T_c = 0.19396$			
0.147	1.04342	1.1213025	-0.000836846	0.186	1.038	1.3917389	-0.000495416
0.148	1.04386	1.1213020	-0.000837338	0.187	1.03831	1.3917386	-0.00049562
0.15	1.04475	1.1213009	-0.000838189	0.189	1.03893	1.3917379	-0.000496039
0.151	1.0452	1.1213004	-0.000838626	0.19	1.03924	1.3917376	-0.000496254
0.152	1.04565	1.1212999	-0.000839073	0.192	1.03987	1.3917370	-0.000496693
0.153	1.0461	1.1212994	-0.000839529	0.193	1.04018	1.3917366	-0.000496918
0.154	6.40615	1.3714	-0.333767	0.194	5.75112	1.66464	-0.32498
0.155	6.60836	1.39186	-0.348736	0.195	5.93915	1.68902	-0.341193
0.156	6.79092	1.41068	-0.362201	0.196	6.10246	1.71065	-0.355221
0.157	6.95969	1.42836	-0.374608	0.197	6.24999	1.73053	-0.367852
0.158	7.11811	1.44519	-0.38622	0.199	6.51421	1.76691	-0.390373
0.16	7.41211	1.47698	-0.407682	0.2	6.63541	1.78391	-0.400662
$d = 10; P = 0.0491927$ and $T_c = 0.235953$				$d = 11; P = 0.0678928$ and $T_c = 0.278925$			
0.227	1.03404	1.6676469	-0.000292273	0.271	1.03123	1.9497594	-0.000176416
0.23	1.03473	1.6676445	-0.000292587	0.272	1.0314	1.9497558	-0.000176466
0.232	1.03519	1.6676429	-0.000292802	0.274	1.03176	1.9497487	-0.000176568
0.233	1.03543	1.6676421	-0.000292912	0.276	1.03212	1.9497416	-0.000176673
0.234	1.03566	1.6676413	-0.000293024	0.277	1.0323	1.9497380	-0.000176727
0.235	1.03589	1.6676405	-0.000293137	0.278	1.03248	1.9497344	-0.000176781

Table 1 continued

T	r_H	ω_r	ω_{im}	T	r_H	ω_r	ω_{im}
0.236	5.40433	1.97324	-0.324694	0.279	5.14764	2.28145	-0.322498
0.237	5.56862	1.99944	-0.340532	0.28	5.29436	2.30916	-0.337921
0.238	5.70992	2.02246	-0.354105	0.281	5.41956	2.33331	-0.351036
0.239	5.83679	2.04349	-0.366254	0.282	5.53144	2.35526	-0.362723
0.24	5.95353	2.06313	-0.3774	0.283	5.63404	2.37569	-0.37341
0.242	6.16581	2.09951	-0.39759	0.284	5.7297	2.39498	-0.383349

while the black hole temperature reads

$$T = \frac{f'(r_H)}{4\pi} = \frac{d-3}{4\pi r_H} \left(1 - \frac{q^2}{r_H^{2(d-3)}} + \frac{d-1}{d-3} \frac{r_H^2}{l^2} \right), \quad (8)$$

where the position of the black hole event horizon, r_H , is determined by solving the condition $f(r = r_H) = 0$ and we choose the largest real positive root. The electric potential Φ measured at infinity with respect to the horizon while the black hole entropy S , was determined from the Bekenstein–Hawking formula ($S = \frac{A_{d-2}}{4}$) [48]. They are given by

$$\Phi = \sqrt{\frac{d-2}{2(d-3)}} \frac{q}{r_H^{d-3}}, \quad (9)$$

$$S = \frac{\omega_{d-2} r_H^{d-2}}{4}. \quad (10)$$

All these quantities satisfy the Smarr formula

$$M = \frac{d-2}{d-3} TS + \Phi Q - \frac{2}{d-3} VP, \quad (11)$$

where the black hole mass M is identified with the enthalpy rather than the internal energy of the gravitational system [30], so the first law of black hole thermodynamics reads [49, 50]

$$dM = TdS + \Phi dQ + VdP. \quad (12)$$

From Eq. (8), one can derive the following equation of state $P = P(r_H, T)$ for a charged AdS black hole in arbitrary dimension d :

$$P = \frac{T(d-2)}{4r_H} - \frac{(d-3)(d-2)}{16\pi r_H^2} + \frac{q^2(d-3)(d-2)}{16\pi r_H^{2(d-2)}}. \quad (13)$$

As usual, the critical points occur when P has an inflection point,

$$\frac{\partial P}{\partial r_H} \Big|_{T=T_c, r_H=r_c} = \frac{\partial^2 P}{\partial r_H^2} \Big|_{T=T_c, r_H=r_c} = 0, \quad (14)$$

leading to

$$\begin{aligned} r_c &= \frac{2((d-2)(2d-5)q^2)^{\frac{1}{2(d-3)}}}{d-2}, \\ T_c &= \frac{(d-3)^2 ((d-2)(2d-5)q^2)^{\frac{1}{6-2d}}}{\pi(2d-5)}, \\ P_c &= \frac{(d-3)^2 ((d-2)(2d-5)q^2)^{\frac{1}{3-d}}}{16\pi}. \end{aligned} \quad (15)$$

As to the Gibbs free energy $G = M - TS$ [48, 51, 52], for fixed charge, it reads [31]

$$G = G(P, T) = \frac{\omega_{d-2}}{16\pi} \left(r_H^{d-3} - \frac{16\pi P r_H^{d-1}}{(d-1)(d-2)} + \frac{(2d-5)q^2}{r_H^{d-3}} \right). \quad (16)$$

After having briefly introduced the main thermodynamical quantities and related phase transition, let us focus our attention in the next section on the derivation of the quasi-normal frequencies of a scalar perturbation around a charged AdS black hole in high dimension spacetime.

3 Master equation in high dimension RN–AdS black hole spacetime

In the sequel, we study the evolution of a massless scalar field in the background of high dimensional charged AdS black hole. The radial part of the field, $\Phi(r, t) = \phi(r)e^{-i\omega t}$, obeys the Klein–Gordon wave equation,

$$\frac{1}{\sqrt{-g}} \partial_\mu (\sqrt{-g} g^{\mu\nu} \partial_\nu \Phi(t, r)) = 0, \quad (17)$$

where $g_{\mu\nu}$ are the covariant metric components of the RN–AdS spacetime, $g^{\mu\nu}$ are the contravariant metric components and g is the metric determinant. The radial functions $\psi(r)$ obey the following differential equation:

$$\phi''(r) + \left[\frac{f'(r)}{f(r)} + \frac{d-2}{r} \right] \phi'(r) + \frac{\omega^2 \phi(r)}{f(r)^2} = 0, \quad (18)$$

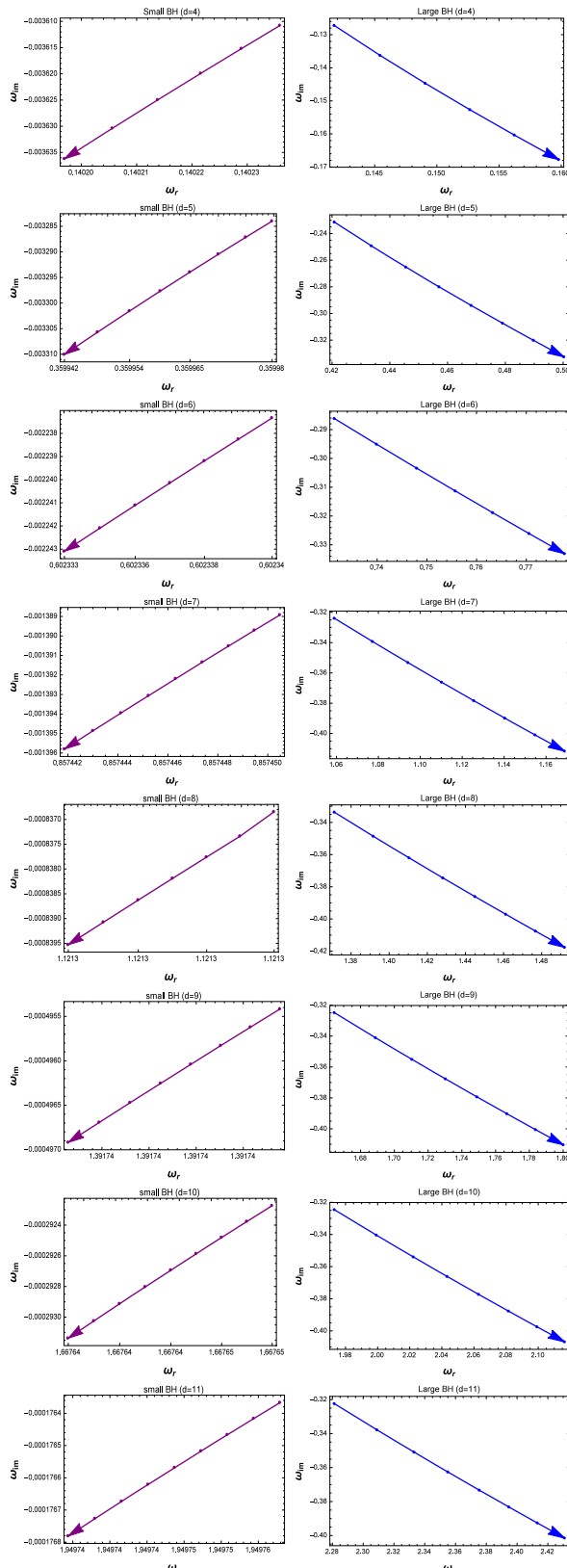


Fig. 2 The behavior of the quasinormal modes for small and large black holes in the complex- ω plane for $4 \leq d \leq 11$. The increase of the black hole size is shown by the arrows for the isobaric process

where ω are complex numbers $\omega = \omega_r + i\omega_{im}$, corresponding to the QNM frequencies of the oscillations describing the perturbation. Notice that the imaginary part ω_{im} must be negative since the QNMs decay in time.

Defining $\phi(r)$ as $\psi(r) \exp[-i \int \frac{\omega}{f(r)} dr]$, then in the vicinity of the black hole horizon r_H , the exponential simplifies to

$$\exp \left[-i \int \frac{\omega}{f(r)} dr \right] \sim (r - r_H)^{-i \frac{\omega}{4\pi T}}, \quad (19)$$

and the incoming waves behave as $\psi(r) \sim (r - r_H)^{-i \frac{\omega}{4\pi T}}$, which means that $\psi(r)$ is set to unity at the horizon [1]. Then we can reformulate Eq. (18) as

$$\psi''(r) + \psi'(r) \left[\frac{f'(r)}{f(r)} - \frac{2i\omega}{f(r)} + \frac{d-2}{r} \right] - \psi(r) \frac{(d-2)i\omega}{rf(r)} = 0. \quad (20)$$

At this stage, for computation reasons, we use the coordinate transformation $u = (\frac{r_H}{r})^{d-3}$, so the AdS boundary is located at $u = 0$, while the horizon is located at $u = 1$. In this case, Eq. (20) becomes

$$\begin{aligned} \psi''(u) + & \left[\frac{f'(u)}{f(u)} + \frac{2i\omega r_H}{(d-3)u^{\frac{d-2}{d-3}} f(u)} \right] \psi'(u) \\ & - \frac{(d-2)i\omega r_H}{(d-3)^2 u^{\frac{2d-5}{d-3}} f(u)} \psi(u) = 0, \end{aligned} \quad (21)$$

with $\psi(u) = 0$ at the AdS limit $u \rightarrow 0$. Thanks to the boundary conditions, we can solve numerically Eq. (21) and find out the frequencies of the quasinormal modes via the shooting method; see for example [53, 54].

The main purpose of the present paper is to show that the dynamical behavior of the quasinormal modes in the massless scalar perturbation encodes the signature of a thermodynamical first-order phase transition of high dimensions charged AdS black holes. The isobaric and the isothermal processes are used to perform this analysis in the context of the van der Waals phase transition picture.

4 QNM behaviors in the isobaric phase transition

Since the pressure P (or cosmological constant Λ) is fixed in an isobaric phase transition, the horizon radius r_H is the only variable in the system. Our subsequent analysis will take into account the spacetime dimension.

In Fig. 1, we show the behavior of this transformation in (T, r_H) -diagram for $d = 4$ and $d = 6$.

From the top panel of Fig. 1, we can see small-large black hole phase transitions under the critical regime $P < P_c$ (solid lines) and at $P = P_c$ (dashed lines), for which the coordinates of the critical point (T_c, r_{Hc}) are determined by the roots of

Table 2 The quasinormal frequencies of the massless scalar perturbation as a function of the black holes temperature for the second phase transition. The upper part, above the horizontal lines is for the small black hole phase while the lower part is for the large one

T	r_H	ω_r	ω_{im}	T	r_H	ω_r	ω_{im}
$d = 4; P = \frac{1}{96\pi}; T_c = \frac{1}{3\sqrt{6}\pi}$				$d = 5; P = \frac{1}{4\sqrt{15}\pi}; T_c = \frac{4}{5\sqrt[4]{15}\pi}$			
0.04325	2.12921	0.373656	-0.16243	0.12900	1.70305	1.09899	-0.330669
0.04326	2.14449	0.373834	-0.16348	0.12905	1.71328	1.1	-0.332973
0.04327	2.16191	0.374037	-0.16468	0.12915	1.73767	1.10244	-0.338505
0.04328	2.18232	0.374277	-0.166092	0.12920	1.75278	1.10396	-0.34196
0.04330	2.24036	0.374969	-0.170132	0.12925	1.7711	1.10583	-0.346171
0.04331	2.2935	0.375616	-0.173864	0.12935	1.83052	1.11201	-0.360003
0.04332	2.46519	0.37781	-0.186085	0.12940	1.99776	1.13047	-0.399977
0.04342	2.91401	0.384421	-0.218748	0.13040	2.4749	1.19173	-0.51797
0.04352	3.05536	0.386788	-0.22915	0.13140	2.6437	1.21623	-0.560176
0.04362	3.16044	0.388638	-0.236902	0.13190	2.71167	1.22648	-0.577182
0.04372	3.24776	0.390234	-0.243353	0.13290	2.8304	1.24487	-0.606881
0.04442	3.67289	0.398748	-0.274831	0.13390	2.93431	1.26146	-0.632857
$d = 6; P = \frac{9}{16 \cdot 2^{2/3} \sqrt[3]{7}\pi}; T_c = \frac{9}{7\sqrt[3]{2} \sqrt[6]{7}\pi}$				$d = 7; P = \frac{1}{\sqrt{3} \sqrt[4]{5}\pi}; T_c = \frac{16}{9\sqrt[4]{3} \sqrt[8]{5}\pi}$			
0.234	1.52352	1.94478	-0.443003	0.35100	1.45959	2.85865	-0.536049
0.2341	1.53118	1.94674	-0.446029	0.35110	1.46711	2.86218	-0.540292
0.2342	1.53965	1.94893	-0.449393	0.35130	1.48616	2.87124	-0.551117
0.2343	1.54916	1.9514	-0.45319	0.35140	1.49925	2.87755	-0.558612
0.2345	1.57293	1.95764	-0.462758	0.35150	1.5177	2.88656	-0.569251
0.2347	1.61025	1.96766	-0.477988	0.35160	1.55588	2.90562	-0.591485
0.23536	1.98703	2.08269	-0.639254	0.35262	1.84354	3.0654	-0.76382
0.23586	2.06224	2.1084	-0.672126	0.35362	1.91764	3.11066	-0.808672
0.23686	2.16511	2.14489	-0.717154	0.35562	2.02036	3.17581	-0.870795
0.23786	2.24312	2.17352	-0.751302	0.35762	2.09921	3.22758	-0.918385
0.23886	2.30893	2.19827	-0.78009	0.35862	2.13387	3.2508	-0.939268
0.23986	2.3672	2.22063	-0.805557	0.35962	2.16632	3.27277	-0.958793
$d = 8; P = \frac{25}{16 \sqrt[5]{66}\pi}; T_c = \frac{25}{11 \sqrt[10]{66}\pi}$				$d = 9; P = \frac{9}{4\sqrt[6]{9}\pi}; T_c = \frac{36}{13 \sqrt[12]{9}\pi}$			
0.47500	1.39001	3.78601	-0.585056	0.60440	1.34473	4.73053	-0.620012
0.47510	1.39486	3.78939	-0.588465	0.60470	1.35759	4.74264	-0.630635
0.47530	1.40632	3.79744	-0.596561	0.60480	1.36299	4.74778	-0.635122
0.47550	1.42172	3.8084	-0.607515	0.60490	1.36931	4.75381	-0.64038
0.47560	1.4323	3.81603	-0.615092	0.60500	1.37699	4.76121	-0.646801
0.47580	1.47862	3.85022	-0.648617	0.60520	1.40253	4.78622	-0.668309
0.47682	1.70606	4.03586	-0.817452	0.60578	1.5752	4.96978	-0.816938
0.47882	1.80802	4.12734	-0.893694	0.60628	1.61091	5.01058	-0.847944
0.47982	1.84462	4.16127	-0.921023	0.60728	1.65914	5.06706	-0.889822
0.48082	1.87682	4.19156	-0.945042	0.60828	1.69526	5.11035	-0.921164
0.48282	1.93286	4.24525	-0.986773	0.60878	1.71091	5.12935	-0.934735
0.48482	1.9817	4.29298	-1.02305	0.60978	1.73907	5.16393	-0.959132
$d = 10; P = \frac{49}{16 \cdot 2^{3/7} \sqrt[7]{15}\pi}; T_c = \frac{49/15\pi}{2^{3/14} \sqrt[14]{15}}$				$d = 11; P = \frac{4}{\sqrt[4]{3} \sqrt[8]{17}\pi}; T_c = \frac{64/17}{8\sqrt[3]{16} \sqrt[16]{17}\pi}$			
0.73800	1.31927	5.69393	-0.65132	0.87000	1.23095	6.56975	-0.605915
0.73820	1.32833	5.70477	-0.659784	0.87100	1.23882	6.58022	-0.613562
0.73830	1.33403	5.71163	-0.665122	0.87200	1.24843	6.59318	-0.623001
0.73840	1.34104	5.72015	-0.671723	0.87300	1.26096	6.61033	-0.635443
0.73850	1.35046	5.73168	-0.680613	0.87400	1.27963	6.63642	-0.654244

Table 2 continued

T	r_H	ω_r	ω_{im}	T	r_H	ω_r	ω_{im}
0.73860	1.3662	5.75121	-0.695545	0.87500	1.33188	6.71262	-0.707968
0.73966	1.54076	5.98629	-0.864036	0.87606	1.48657	6.96169	-0.870845
0.74166	1.61302	6.09234	-0.934128	0.87706	1.52291	7.02465	-0.909279
0.74366	1.66147	6.16595	-0.98104	0.87806	1.55006	7.07268	-0.937969
0.74566	1.70076	6.22703	-1.019	0.88006	1.59256	7.14948	-0.982812
0.74766	1.73487	6.281	-1.05188	0.88206	1.62697	7.21305	-1.01905
0.74866	1.75057	6.30612	-1.06699	0.88306	1.64234	7.24183	-1.03521

the system: $\frac{\partial T}{\partial r_H} = \frac{\partial^2 T}{\partial r_H^2} = 0$. The Gibbs free energy displays a characteristic swallow tail behavior, depicted in the bottom panel (solid lines), signaling a first-order SBH/LBH phase transition. The dashed line indicates the character of a second-order phase transition due a continuous variation of the free energy between SBH and LBH.

Table 1 lists the frequencies of the quasinormal modes of the massless scalar perturbation around small and large black holes for the first-order phase transition where the pressure is fixed at the value $P = 0.1 P_c$.

One should keep in mind that, unlike the ordinary normal modes, the QNMs decay at certain rates. Hence, having complex frequencies, the real and imaginary parts can help to gain some insight in the oscillations and decays of the black hole. In the case of the small black hole phase, for any dimension, we note from Table 1 that the black hole becomes smaller and smaller when the temperature decreases from the phase transition critical point T_c . In this process, the real part of the QNMs frequencies varies slightly, while the absolute value of the imaginary part decreases which indicates that the absorption performance of the black hole is reduced whatever the spacetime dimension d is. This result is consistent with the overall analysis reported in [1, 55].

For large black hole phase, for any dimension d , we see that by increasing the temperature from the critical value T_c , the black hole becomes larger. In this case, the real part as well as the absolute value of the imaginary part of the quasinormal frequencies increases. Furthermore, the massless scalar perturbation outside the black hole performs more oscillations but decays faster. These observations are in agreement with the results found in [1, 56].

Using the results of Table 1, we illustrate in Fig. 2 the quasinormal frequencies for small and large black hole phases where the purple (blue) dots correspond to the results of the upper (lower) part, above the horizontal line in Table 1, respectively. The increase in the size of the black hole is indicated by the arrows. Notice here that Fig. 2 corresponds to the solid lines in Fig. 1.

From Fig. 2, we see different slopes of the quasinormal frequencies in the massless scalar perturbations with different

phases of the small and large black holes. The SBH and LBH transform to each other through a phase transition. All these features revealed by dynamical perturbations are concording with the general picture of thermodynamic phase transitions between small-large RN–AdS black holes.

At the isobaric phase transition critical point $P = P_c$, the situation is different. The values of the frequencies are shown in the Table 2.

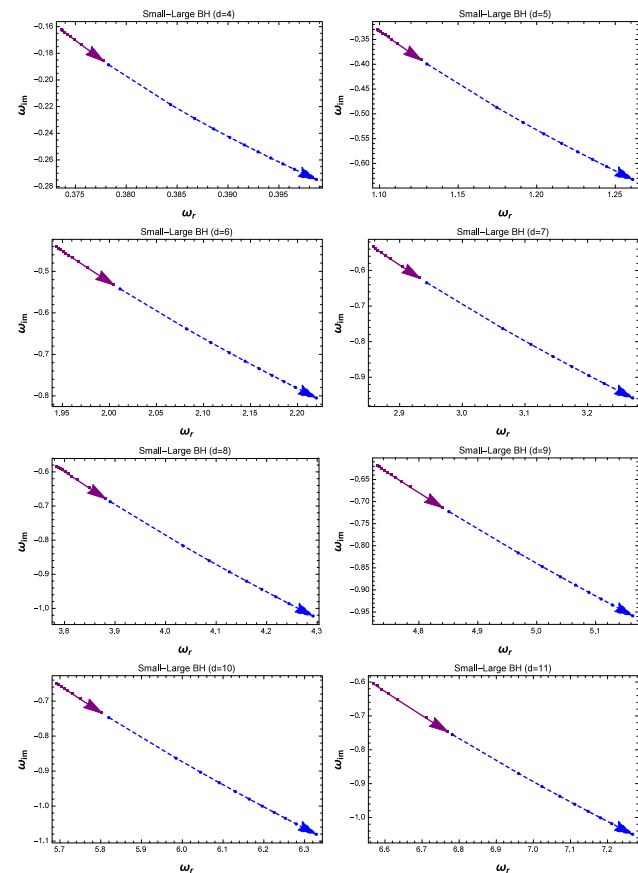


Fig. 3 The behavior of the quasinormal modes for small (solid) and large (dashed) black holes in the isobaric second-order phase transition for a $4 \leq d \leq 11$. The increase of the black hole size is shown by the arrows

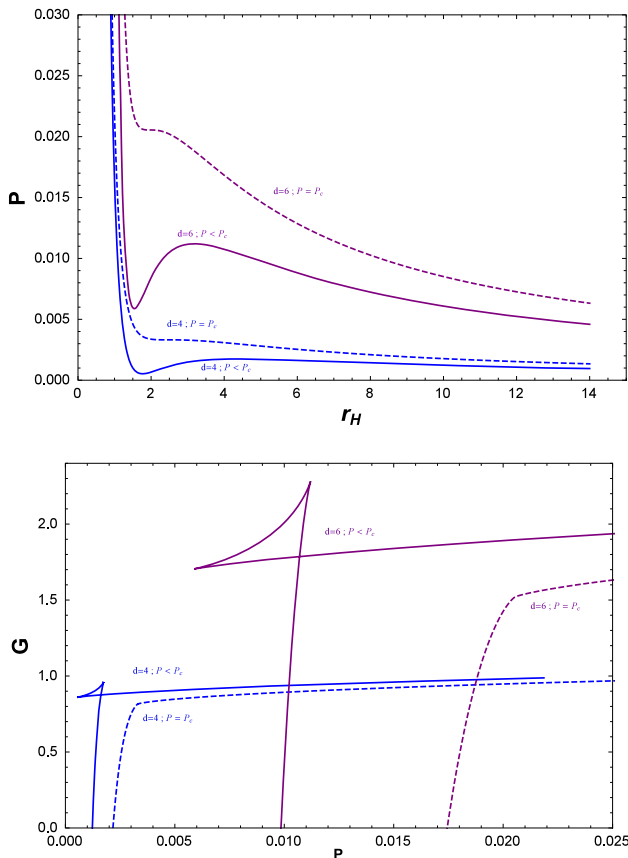


Fig. 4 Left panel pressure P as a function of the horizon radius r_H for isothermal process. Right panel Gibbs free energy as a function of the pressure for $d = 4, 6$. The two upper lines (purple) correspond to $d = 6$ while the lower two lines (blue) correspond to $d = 4$. The critical isotherm $T = T_c$ is denoted by the dashed lines, the solid lines shows the first-order transition $T < T_c$

The quasinormal frequencies for small and large black hole phases illustrated in Table 2 are plotted in Fig. 3 for $4 \leq d \leq 11$, at this level we must stress that this figure corresponds to the dashed lines in the Fig. 1.

We can see that when phase transitions are realized, the SBH and the LBH QNMs have the same behavior when the horizon increases, generalizing to higher spacetime dimensions the property found in $d = 4$ [1].

5 QNM behaviors in the isothermal phase transition

In this section, we fix the temperature T and made the study in the (P, r_H) -diagram. In Fig. 4, we plot the pressure of the black hole in terms of the radius of event horizon and the Gibbs free energy.

The associated (P, r_H) -diagram for $d = 4$ black hole is displayed in Fig. 4 (left panel). Obviously, for $T < T_c$ there

is a small-large black hole phase transition in the system. This qualitative behavior persists in higher dimensions, as illustrated for $d = 6$. In the right panel the behavior of G for dimensions $d = 4$ and $d = 6$ is depicted in Fig. 4. Similarly to Fig. 1, the characteristic first-order phase transition behavior shows up.

Table 3 displays the frequencies of the quasinormal modes for small and large black hole phase in the isothermal process for different dimensions, with $T = 0.74T_c$. The data above (below) the horizontal line are for the small (large) black hole phase, respectively.

From Fig. 5, we can see that the behavior of the quasinormal modes in the isothermal process is not regular and depends on the spacetime dimension. Indeed:

- For $d = 4$ and $d = 5$, we see that, for the SBH phase, the corresponding pressure P decreases with growing black hole horizon. In this process, the real part of the frequencies as well as the absolute imaginary part decrease. For the LBH case, the pressure also decreases when the black hole size increases. However, the real and the absolute values of the imaginary parts have opposite behaviors. Figure 5 shows the behaviors of the quasinormal modes for small and large holes where the arrows indicate increase of the black hole size. It is clear that the remarkable properties of the quasinormal frequencies are completely different in SBH and LBH phases, confirming the behavior seen in $d = 4$ [1], and providing a good measure to probe the black hole phase transitions.
- For $d \geq 6$, the behaviors of QNM in the two black hole phases are completely different: when the horizon radius grows the real and absolute value of the imaginary parts both decrease (increase) in the SBH phase (LBH phase), respectively. Therefore the QNM behavior is sensitive to the dimension d , which affects the correction induced by the variation of the horizon radius r_H and the pressure P , as can be seen from the master equation, Eq. (21).

In the isothermal transition, the quasinormal modes can be affected by the value of the pressure $P(l)$ and the horizon radius r_H . To illustrate the effect of these two parameters, we restrict our calculation here to only $d = 4, d = 5$ and $d = 6$. For higher dimensions, $d > 6$, the behavior is exactly similar to $d = 6$ as shown in Table 4. This feature can also be seen clearly in Fig. 6 where we notice a competition between the pressure P and horizon radius r_H . Each of these parameters aims to overwhelm the other which affects the decay rate of the field, namely ω_i .

Table 3 The QNM frequencies of the massless scalar perturbation for black holes with different dimensions and sizes in the isothermal process

P	r_H	ω_r	ω_{im}	P	r_H	ω_r	ω_{im}
$d = 4; P_c = 0.00157088 \text{ and } T = 0.0320542$				$d = 5; P_c = 0.0103914 \text{ and } T = 0.0957523$			
0.0023	1.32801	0.313337	-0.0766033	0.0135	1.23535	0.8608	-0.138736
0.0021	1.34336	0.301581	-0.0688084	0.013	1.24149	0.845309	-0.131794
0.002	1.35161	0.295472	-0.0649205	0.012	1.2548	0.813519	-0.118079
0.0018	1.36945	0.282723	-0.0571742	0.0115	1.26207	0.79718	-0.111318
0.0017	1.37917	0.276049	-0.0533207	0.011	1.26981	0.780515	-0.104628
0.0016	1.38951	0.269149	-0.0494843	0.0105	1.2781	0.763497	-0.0980188
0.00156	6.36627	0.286755	-0.222296	0.0045	14.074	0.944997	-0.714101
0.0014	7.32754	0.285987	-0.239667	0.004	16.1001	0.944984	-0.728163
0.0013	8.31838	0.284555	-0.253537	0.003	22.141	0.944314	-0.754857
0.0012	9.39777	0.282746	-0.26541	0.002	34.1599	0.942915	-0.779934
0.0011	10.6133	0.280682	-0.275946	0.001	70.1117	0.940907	-0.803661
0.0010	12.0182	0.278429	-0.285503	0.0005	141.947	0.939703	-0.815083
$d = 6; P_c = 0.0306566 \text{ and } T = 0.173793$				$d = 7; P_c = 0.0648614 \text{ and } T = 0.2602$			
0.037	1.18927	1.46326	-0.166943	0.068	1.17485	1.98887	-0.152482
0.035	1.19798	1.42273	-0.153541	0.067	1.17726	1.97383	-0.148805
0.034	1.20266	1.40213	-0.14694	0.0665	1.17849	1.96627	-0.146978
0.033	1.20759	1.38128	-0.140413	0.066	1.17975	1.9587	-0.145159
0.032	1.21278	1.36018	-0.133963	0.0655	1.18103	1.9511	-0.143348
0.031	1.2183	1.3388	-0.127597	0.065	1.18233	1.94348	-0.141544
0.03	3.55703	1.63219	-0.626789	0.064	3.03158	2.37227	-0.700765
0.025	5.06739	1.70814	-0.786255	0.059	3.6804	2.45839	-0.822831
0.02	6.97943	1.74585	-0.891377	0.054	4.31594	2.51127	-0.90842
0.015	9.99367	1.77001	-0.976436	0.049	5.0203	2.55064	-0.978804
0.01	15.8756	1.78665	-1.05007	0.044	5.84492	2.5822	-1.04021
0.005	33.326	1.79836	-1.11605	0.039	6.85048	2.60853	-1.0955
$d = 8; P_c = 0.114605 \text{ and } T = 0.352107$				$d = 9; P_c = 0.180982 \text{ and } T = 0.447907$			
0.117	1.15334	2.60132	-0.154053	0.183	1.13575	3.23913	-0.154243
0.1162	1.15443	2.59209	-0.152204	0.1824	1.13625	3.23358	-0.1533
0.116	1.1547	2.58977	-0.151743	0.182	1.13659	3.22989	-0.152672
0.1154	1.15553	2.58283	-0.150363	0.1814	1.1371	3.22433	-0.151733
0.115	1.1561	2.5782	-0.149446	0.1812	1.13727	3.22248	-0.151421
0.1148	1.15638	2.57588	-0.148988	0.181	1.13744	3.22063	-0.151108
0.114	2.67852	3.10198	-0.727098	0.18	2.49165	3.84363	-0.750582
0.109	3.05069	3.19286	-0.827744	0.175	2.73034	3.92879	-0.83067
0.104	3.38124	3.25244	-0.899785	0.17	2.93771	3.98859	-0.890562
0.099	3.71	3.29864	-0.959385	0.16	3.33138	4.07696	-0.98509
0.089	4.41574	3.36992	-1.05857	0.15	3.73361	4.14414	-1.06217
0.079	5.24526	3.42501	-1.1421	0.14	4.16632	4.19932	-1.12918
$d = 10; P_c = 0.264781 \text{ and } T = 0.546605$				$d = 11; P_c = 0.366593 \text{ and } T = 0.647545$			
0.267	1.12144	3.89469	-0.153065	0.368	1.11035	4.55202	-0.149345
0.266	1.12199	3.88705	-0.151936	0.3676	1.11051	4.54943	-0.149007
0.2658	1.1221	3.88552	-0.15171	0.3672	1.11066	4.54683	-0.148671
0.2654	1.12232	3.88246	-0.15126	0.367	1.11074	4.54554	-0.148502
0.265	1.12254	3.8794	-0.15081	0.3668	1.11081	4.54424	-0.148334
0.2648	1.12266	3.87787	-0.150586	0.3666	1.11089	4.54294	-0.148166
0.26	2.46955	4.63737	-0.806927	0.365	2.23893	5.30884	-0.758411
0.25	2.75572	4.75123	-0.90625	0.36	2.36416	5.3839	-0.814212
0.24	3.01582	4.8317	-0.981443	0.355	2.47173	5.44066	-0.858141
0.23	3.27327	4.89615	-1.04485	0.35	2.57093	5.48771	-0.895714
0.22	3.53769	4.95073	-1.1009	0.34	2.75731	5.56482	-0.959642
0.215	3.67449	4.97533	-1.12689	0.33	2.93736	5.62801	-1.01428

To illustrate how these two factors affect the quasinormal frequencies, we perform a double-series expansion of the frequency $\omega(r_H + \Delta r_H, P + \Delta P)$ [1]:

$$\begin{aligned} \omega(r_H + \Delta r_H, P + \Delta P) &= \omega(r_H, P) + \frac{\partial \omega}{\partial r_H} \Delta r_H + \frac{\partial \omega}{\partial P} \Delta P \\ &\quad + \mathcal{O}(\Delta r_H^2, \Delta P^2, \Delta r_H \cdot \Delta P), \end{aligned} \quad (22)$$

with

$$\tilde{\omega} = \omega + \Delta r_H + \Delta p + \mathcal{O}(\Delta r_H^2, \Delta P^2, \Delta r_H \cdot \Delta P),$$

where Δr_H and Δp represent corrections induced by variation of the black hole size and pressure, respectively. Recall here that the choice of the step of pressure ΔP in a linear approximation is related to Δr_H via the relation

$$\begin{aligned} dP = & \left(-\frac{(d-2)T}{4r_H^2} + \frac{(3-d)(d-2)^2 r_H^{(3-2d)}}{8\pi} \right. \\ & \left. + \frac{(d-3)(d-2)}{8\pi r_H^3} \right) dr_H. \end{aligned} \quad (23)$$

Table 5 shows the evaluation of the quasinormal frequencies $\tilde{\omega}$ from the linear approximation for small and large black hole phase (this evaluation is performed in a narrow range of r_H in order to preserve the linear approximation in Eq. (23)). One can see that the behaviors of $\tilde{\omega}$ are consistent with the numerical computation. For example for a small black hole at $d = 5$ we obtain $\tilde{\omega}_r < \omega_r$ and $|\tilde{\omega}_{im}| < |\omega_{im}|$, which confirms the behavior shown in Fig. 5.

It is clear that, for the small black hole case and for all dimensions, the change of the pressure prevails over the change of the black hole size. We also notice that the imaginary part of the frequency is more sensitive to the pressure.

The quasinormal frequencies for small and large black hole phases are plotted in Fig. 7 for $4 \leq d \leq 11$. For the isothermal phase transition at $T = T_c$, we can see that when phase transitions are realized, the SBH and the LBH QNMs have the same behavior as the horizon increases, which generalizes the result of [1] to higher dimensional spacetime.

6 Critical ratio and the detection efficiency

From the previous sections we can see that the quasinormal normal mode frequencies provide an efficient investigating tool to probe the signature of the black hole phase transition. The critical ratio parameter defined by $\chi = \frac{P}{P_c}$ plays a prominent role in this detection. To illustrate how this parameter affects the way how quasinormal frequencies can be a good measure to probe different phases of the black hole,

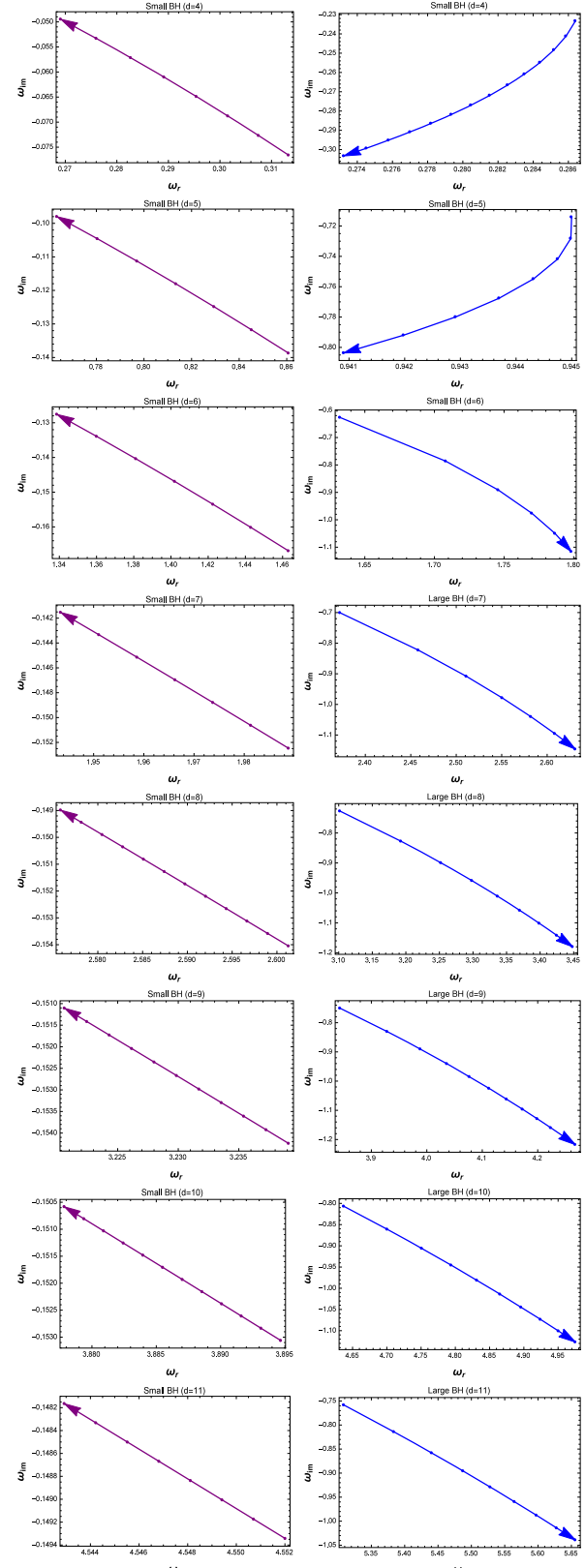


Fig. 5 The behavior of the quasinormal modes for small and large black holes for a $4 \leq d \leq 11$. The increase in the black hole size is shown by arrows in the case of the isothermal process

Table 4 Left: the quasinormal frequencies as a function of the black hole horizon r_H , for fixed pressure P . Right: quasinormal frequencies as a function of P , for fixed black hole horizons r_H

P	r_H	ω_r	ω_{im}	r_H	P	ω_r	ω_{im}
Small BH ($d = 4$)							
0.002	1.32238	0.295522	-0.0643022	1.352	0.00201306	0.296278	-0.0654519
	1.35161	0.295472	-0.0649205		0.00200653	0.295875	-0.0651862
	1.38539	0.295434	-0.065692		0.002	0.295472	-0.0649205
	1.42549	0.295411	-0.0666873		0.00199347	0.295068	-0.0646549
	1.47507	0.295403	-0.0680322		0.00198694	0.294664	-0.0643894
Large BH ($d = 4$)							
0.0014	7.78691	0.283655	-0.244264	7.914	0.00141306	0.286948	-0.250613
	7.85092	0.284421	-0.246286		0.00140653	0.286066	-0.249448
	7.91417	0.285183	-0.248283		0.0014	0.285183	-0.248283
	7.9767	0.285942	-0.250256		0.00139347	0.2843	-0.247118
	8.03854	0.286699	-0.252208		0.00138694	0.283416	-0.245953
Small BH ($d = 5$)							
0.012	1.23887	0.8133	-0.117003	1.255	0.0132254	0.852622	-0.136113
	1.24662	0.813403	-0.117518		0.0126127	0.833267	-0.127053
	1.2548	0.813519	-0.118079		0.012	0.813519	-0.118079
	1.26348	0.813648	-0.118692		0.0113873	0.793341	-0.109201
	1.2727	0.813793	-0.119364		0.0107746	0.772694	-0.100431
Large BH ($d = 5$)							
0.003	21.5956	0.924718	-0.735804	22.141	0.00307123	0.964986	-0.772998
	21.8686	0.934517	-0.745342		0.00303561	0.95465	-0.763927
	22.141	0.944314	-0.754857		0.003	0.944314	-0.754857
	22.4128	0.954109	-0.764347		0.00296439	0.933977	-0.745786
	22.684	0.963901	-0.773816		0.00292877	0.923639	-0.736716
Small BH ($d = 6$)							
0.034	1.19496	1.40178	-0.146022	1.203	0.0356841	1.43709	-0.159068
	1.19874	1.40195	-0.146469		0.034842	1.41969	-0.152981
	1.20266	1.40213	-0.14694		0.034	1.40213	-0.14694
	1.20672	1.40232	-0.147438		0.033158	1.38441	-0.140946
	1.21094	1.40252	-0.147965		0.0323159	1.36652	-0.135001
Large BH ($d = 6$)							
0.02	6.84613	1.72298	-0.872432	6.979	0.0202979	1.7678	-0.905398
	6.91299	1.73444	-0.881938		0.0201489	1.75683	-0.898387
	6.97943	1.74585	-0.891377		0.02	1.74585	-0.891377
	7.04545	1.75723	-0.900751		0.0198511	1.73488	-0.884367
	7.11109	1.76858	-0.910063		0.0197021	1.7239	-0.877357

we present a brief analysis for several values of χ parameter: we replot in Fig. 8 the quasinormal frequencies for small and large black hole phases for the isobaric transition using different values of χ .

Therein we can see that, for $\chi = 0.6, 0.9$, $\omega_r - \omega_i$ plane does not show different slope in small and large black hole phases near the critical temperature. In large black hole phase, the quasinormal modes continue to have the same salient feature noticed in the previous sections. However, in the small black hole phase, we clearly observe a change of slope sign around the point dubbed T in the figure.

In Table 6, we show the values of the temperature T corresponding to the slope sign change in the small black hole phase for different values of the critical ratio χ and for the spacetime dimension d .

Here, we need to highlight the following issue: when the critical ratio χ becomes very small, T tends to the critical temperature and the quantity $\Delta T = T_c - T$ becomes null. On the other hand, the quantity ΔT increases when χ becomes large and the quasinormal modes are not very efficient to probe the black hole phase transition. As in the case of the second phase transition we also should mention that, since

Fig. 6 The purple dashed plots show the quasinormal frequencies variation with the horizon r_H , for fixed pressure P . The blue dots represent the quasinormal frequencies as a function of P , for fixed black hole horizons r_H (Table 4). The arrow indicates the increase of r_H (P) for fixed P (r_H), respectively

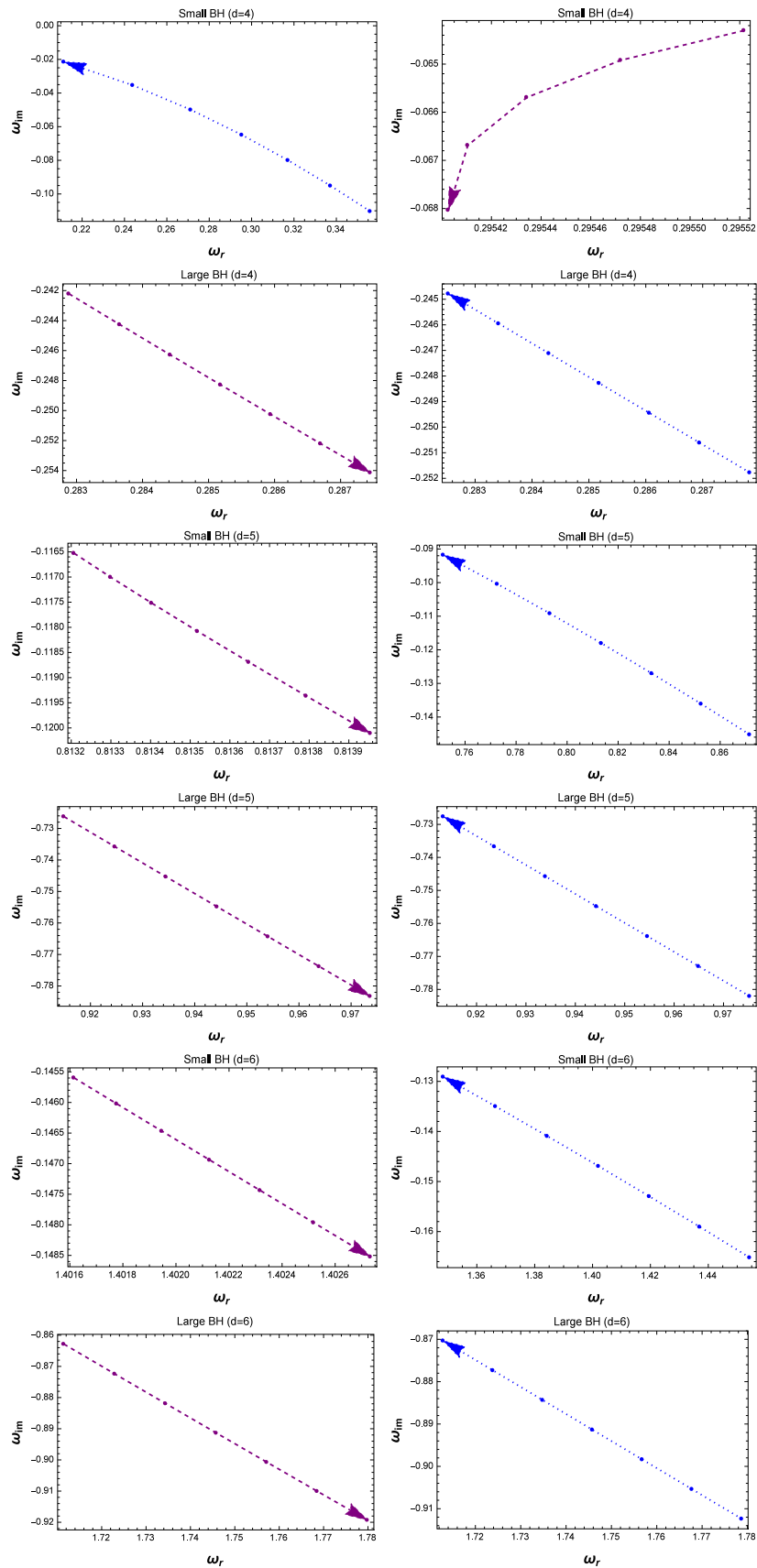


Table 5 $\tilde{\omega}$ is the quasinormal frequency from the linear approximation. Δ_{r_H} and Δ_p represent corrections due to variation of the black hole size and pressure, respectively

P	r_H	ω	$\tilde{\omega}$	Δ_{r_H}	Δ_p
Small BH ($d = 4$)					
0.002	1.352	0.295472–0.0649205 i	0.289516–0.0611853 i	-0.00594507+0.00391361 i	-0.0000114725–0.000178387 i
0.0019	1.360	0.289191–0.0610417 i	0.283101–0.05734 i	-0.00607645+0.00388441 i	-0.0000133426–0.00018272 i
0.0017	1.379	0.276049–0.0533207 i	0.269655–0.0496962 i	-0.00637566+0.00381701 i	-0.0000186237–0.000192563 i
Large BH ($d = 4$)					
0.0014	7.914	0.285183–0.248283 i	0.284939–0.250513 i	-0.00222237+0.00293185 i	0.00197779–0.005162 i
0.00135	8.422	0.284389–0.254799 i	0.284128–0.256734 i	-0.00219918+0.00292837 i	0.00193895–0.00486306 i
0.0013	8.952	0.283505–0.260848 i	0.283237–0.262547 i	-0.00217896+0.00292535 i	0.00191109–0.00462342 i
Small BH ($d = 5$)					
0.013	1.241	0.845309–0.131794 i	0.840402–0.129622 i	-0.00494032+0.00231399 i	0.0000336195–0.000141584 i
0.012	1.255	0.813519–0.118079 i	0.808489–0.115967 i	-0.00506175+0.0022644 i	0.000031792–0.000152273 i
0.011	1.270	0.780515–0.104628 i	0.775344–0.102586 i	-0.00519991+0.00220809 i	0.0000287101–0.000165456 i
Large BH ($d = 5$)					
0.004	16.100	0.944984–0.728163 i	0.944981–0.728497 i	-0.00256351+0.00224264 i	0.00256039–0.00257707 i
0.003	22.141	0.944314–0.754857 i	0.944304–0.755084 i	-0.00255623+0.00224307 i	0.00254691–0.00247059 i
0.001	70.112	0.940907–0.803661 i	0.940901–0.803725 i	-0.00254884+0.00224348 i	0.00254249–0.00230779 i
Small BH ($d = 6$)					
0.034	1.203	1.40213–0.14694 i	1.39765–0.145521 i	-0.004582+0.00154515 i	0.0000481149–0.000125901 i
0.033	1.208	1.38128–0.140413 i	1.37676–0.139015 i	-0.00456325+0.00152818 i	0.0000477697–0.000130945 i
0.032	1.213	1.36018–0.133963 i	1.35562–0.132589 i	-0.00459992+0.00151046 i	0.0000473116–0.000136514 i
Large BH ($d = 6$)					
0.025	5.067	1.70814–0.786255 i	1.70865–0.787499 i	-0.00278508+0.00174631 i	0.00328594–0.00299044 i
0.02	6.979	1.74585–0.891377 i	1.74607–0.892069 i	-0.00274466+0.0017533 i	0.00296364–0.00244549 i
0.01	15.876	1.78665–1.05007 i	1.78669–1.05029 i	-0.00271047+0.00175882 i	0.00275593–0.00198602 i

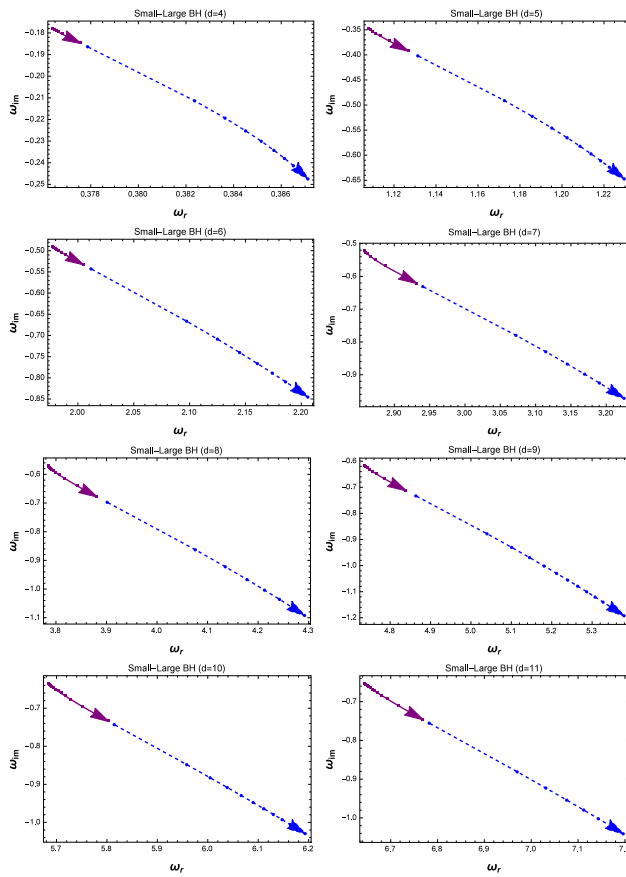


Fig. 7 The behavior of the quasinormal modes for small (solid) and large (dashed) black holes in the isothermal second-order phase transition for a $4 \leq d \leq 11$. The increase in the black hole size is shown by arrows

the quantity ΔT is sensitive to the spacetime dimension, d affects the efficiency of the quasinormal modes detection.

To close, we plot the real part of the quasinormal mode frequencies as a function of the temperature T , Fig. 9, in order to show the dashed region corresponding to the temperature interval where the quasinormal mode frequencies are able to reveal the phase transition.

7 Conclusion

In this work, we have investigated the thermodynamical behaviors of d -dimensional charged AdS black holes and their phase transitions. Emphasis has been put on the calculation of the quasinormal modes frequencies of the massless scalar perturbation around small and large black holes. This study has been performed for an isobaric process as well as isothermal one.

For the former, below the critical pressure, we found that, for any dimension d in the range $4 \leq d \leq 11$, the QNMs might well be an useful tool to probe the black hole phase

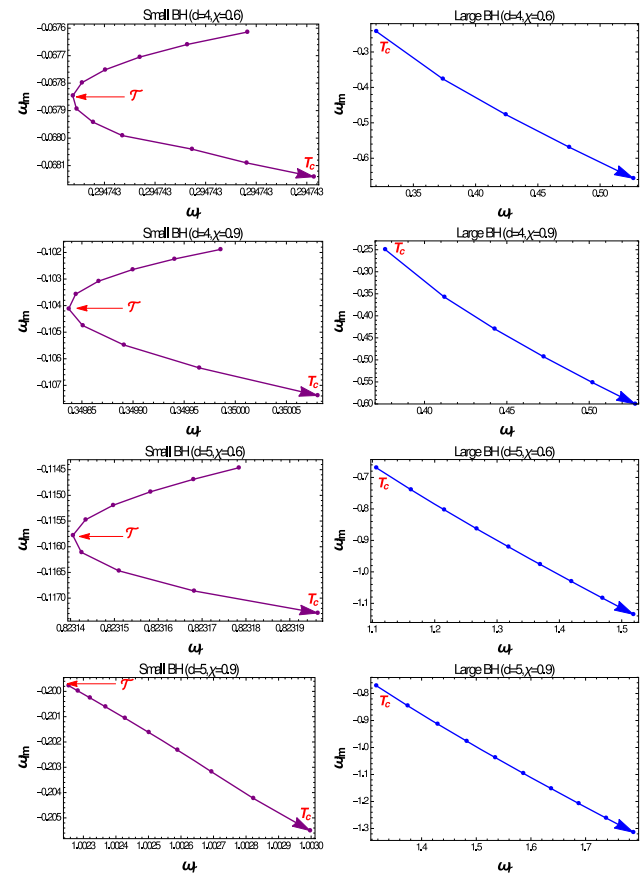


Fig. 8 The quasinormal frequencies in the ω_r – ω_{im} plane for $\chi = 0.6, 0.9$. \mathcal{T} is the temperature corresponding to the slope sign change

Table 6 The temperature \mathcal{T} corresponding to the slope sign change

χ	T_c	\mathcal{T}	ΔT
$d = 4$			
0.1	0.0158676	~0.0158676	~0
0.6	0.0353931	0.0351867	0.000206342
0.9	0.0416175	0.0331899	0.00842754
$d = 5$			
0.6	0.103525	0.0727773	0.0307481
0.65	0.107328	0.0684943	0.0388333
0.9	0.123774	~0	~0.123774

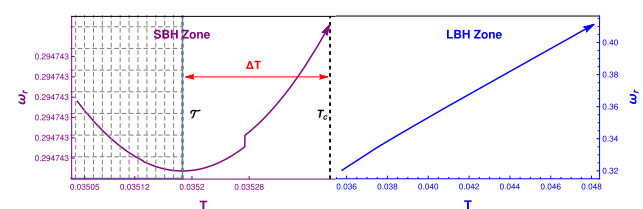


Fig. 9 The real part of the quasinormal modes frequencies as a function of the black hole temperature, with $\chi = 0.6$ and $d = 4$

transition, since the slopes of the quasinormal frequency change between small and large black holes, which can be affected by the value of the critical ratio χ . As to the latter process, for the phase transition below the critical point, we have shown that the spacetime dimension affects the behavior of QNMs. More precisely, we found that the change in QNM slopes occurs only for $d = 4$ and $d = 5$.

Finally we have also found that, at the critical isothermal and isobaric phase transitions, quasinormal frequencies of small and large black holes have the same behavior, suggesting that quasinormal modes are not appropriate to probe the black hole phase transition in the second order.

Acknowledgements This work is supported in part by the Groupement de recherche international (GDRI): Physique de l'infiniment petit et de l'infiniment grand—P2IM. SI would like to thank Prof. S. Mahapatra for providing a code to cross-check the calculations.

Open Access This article is distributed under the terms of the Creative Commons Attribution 4.0 International License (<http://creativecommons.org/licenses/by/4.0/>), which permits unrestricted use, distribution, and reproduction in any medium, provided you give appropriate credit to the original author(s) and the source, provide a link to the Creative Commons license, and indicate if changes were made.

Funded by SCOAP³.

References

- Y. Liu, D.C. Zou, B. Wang, Signature of the Van der Waals like small-large charged AdS black hole phase transition in quasinormal modes. *JHEP* **1409**, 179 (2014). [arXiv:1405.2644](https://arxiv.org/abs/1405.2644)
- C.V. Vishveswara, Scattering of gravitational radiation by a Schwarzschild black-hole. *Nature* **227**, 936 (1970)
- C.V. Vishveswara, Stability of the Schwarzschild metric. *Phys. Rev. D* **1**, 2870 (1970)
- H.P. Nollert, Topical review: quasinormal modes: the characteristic ‘sound’ of black holes and neutron stars. *Class. Quant. Grav.* **16**, R159 (1999)
- E. Berti, V. Cardoso, A.O. Starinets, Quasinormal modes of black holes and black branes. *Class. Quant. Grav.* **26**, 163001 (2009). [arXiv:0905.2975](https://arxiv.org/abs/0905.2975)
- B.P. Abbott et al. [LIGO Scientific and Virgo Collaborations], Observation of gravitational waves from a binary black hole merger. *Phys. Rev. Lett.* **116**, 061102 (2016). [arXiv:1602.03837](https://arxiv.org/abs/1602.03837)
- B.P. Abbott et al., [LIGO Scientific Collaboration], LIGO: the laser interferometer gravitational-wave observatory. *Rep. Prog. Phys.* **72**, 076901 (2009). [arXiv:0711.3041](https://arxiv.org/abs/0711.3041)
- T. Accadia et al., Status of the Virgo project. *Class. Quant. Grav.* **28**, 114002 (2011)
- K. Somiya [KAGRA Collaboration], Detector configuration of KAGRA—the Japanese cryogenic gravitational-wave detector. *Class. Quant. Grav.* **29**, 124007 (2012). [arXiv:1111.7185](https://arxiv.org/abs/1111.7185)
- M. Armano et al., Sub-femto-g free fall for space-based gravitational wave observatories: LISA pathfinder results. *Phys. Rev. Lett.* **116**(23), 231101 (2016)
- J.M. Maldacena, The large N limit of superconformal field theories and supergravity. *Int. J. Theor. Phys.* **38**, 1113 (1999)
- J.M. Maldacena, *Adv. Theor. Math. Phys.* **2**, 231 (1998). [arXiv:hep-th/9711200](https://arxiv.org/abs/hep-th/9711200)
- E. Witten, Anti-de Sitter space, thermal phase transition, and confinement in gauge theories. *Adv. Theor. Math. Phys.* **2**, 505 (1998)
- V. Cardoso, Á.S.J.C. Dias, G.S. Hartnett, L. Lehner, J.E. Santos, Holographic thermalization, quasinormal modes and superradiance in Kerr–AdS. *JHEP* **1404**, 183 (2014). [arXiv:1312.5323](https://arxiv.org/abs/1312.5323)
- V. Cardoso, R. Konoplya, J.P.S. Lemos, Quasinormal frequencies of Schwarzschild black holes in Anti-de Sitter space-times: a complete study on the asymptotic behavior. *Phys. Rev. D* **68**, 044024 (2003). [arXiv:gr-qc/0305037](https://arxiv.org/abs/gr-qc/0305037)
- C.M. Warnick, On quasinormal modes of asymptotically Anti-de Sitter black holes. *Commun. Math. Phys.* **333**, 959 (2015). [arXiv:1306.5760](https://arxiv.org/abs/1306.5760)
- R.A. Konoplya, Decay of charged scalar field around a black hole: quasinormal modes of R–N, R–N–AdS black hole. *Phys. Rev. D* **66**, 084007 (2002). [arXiv:gr-qc/0207028](https://arxiv.org/abs/gr-qc/0207028)
- R.A. Konoplya, A. Zhidenko, Stability of higher dimensional Reissner–Nordström–Anti-de Sitter black holes. *Phys. Rev. D* **78**, 104017 (2008). [arXiv:0809.2048](https://arxiv.org/abs/0809.2048)
- R. Li, H. Zhang, J. Zhao, Time evolutions of scalar field perturbations in D-dimensional Reissner–Nordström Anti-de Sitter black holes. *Phys. Lett. B* **758**, 359 (2016). [arXiv:1604.01267](https://arxiv.org/abs/1604.01267)
- R.A. Konoplya, A. Zhidenko, Quasinormal modes of black holes: from astrophysics to string theory. *Rev. Mod. Phys.* **83**, 793 (2011). [arXiv:1102.4014](https://arxiv.org/abs/1102.4014)
- E. Abdalla, R.A. Konoplya, A. Zhidenko, Perturbations of Schwarzschild black holes in laboratories. *Class. Quant. Grav.* **24**, 5901 (2007). [arXiv:0706.2489](https://arxiv.org/abs/0706.2489) [hep-th]
- R.A. Konoplya, A. Zhidenko, Stability of multidimensional black holes: complete numerical analysis. *Nucl. Phys. B* **777**, 182 (2007). [arXiv:hep-th/0703231](https://arxiv.org/abs/hep-th/0703231) [hep-th]
- A. Zhidenko, Quasinormal modes of brane-localized standard model fields in Gauss–Bonnet theory. *Phys. Rev. D* **78**, 024007 (2008). [arXiv:0802.2262](https://arxiv.org/abs/0802.2262) [gr-qc]
- E. Abdalla, C.B.M.H. Chirenti, A. Saa, Quasinormal mode characterization of evaporating mini black holes. *JHEP* **0710**, 086 (2007). doi:10.1088/1126-6708/2007/10/086. [arXiv:gr-qc/0703071](https://arxiv.org/abs/gr-qc/0703071)
- A. Dabholkar, S. Nampuri, Lectures on quantum black holes. *Lect. Notes Phys.* **851**, 165 (2012)
- S.J. Rey, String theory on thin semiconductors: holographic realization of Fermi points and surfaces. *Prog. Theor. Phys. Suppl.* **177**, 128 (2009)
- H. Witek, H. Okawa, V. Cardoso, L. Gualtieri, C. Herdeiro, M. Shibata, U. Sperhake, M. Zilhao, Higher dimensional numerical relativity: code comparison. *Phys. Rev. D* **90**, 084014 (2014). [arXiv:1406.2703](https://arxiv.org/abs/1406.2703)
- D. Kastor, S. Ray, J. Traschen, Enthalpy and the mechanics of AdS black holes. *Class. Quant. Grav.* **26**, 195011 (2009). [arXiv:0904.2765](https://arxiv.org/abs/0904.2765)
- S. Hawking, D.N. Page, Thermodynamics of black holes in Anti-de Sitter space. *Commun. Math. Phys.* **83**, 577 (1987)
- D. Kastor, S. Ray, J. Traschen, Enthalpy and the mechanics of AdS black holes. *Class. Quant. Grav.* **261**, 95011 (2009). [arXiv:0904.2765](https://arxiv.org/abs/0904.2765)
- A. Chamblin, R. Emparan, C. Johnson, R. Myers, Charged AdS black holes and catastrophic holography. *Phys. Rev. D* **60**, 064018 (1999)
- A. Chamblin, R. Emparan, C. Johnson, R. Myers, Holography, thermodynamics, and fluctuations of charged AdS black holes. *Phys. Rev. D* **60**, 104026 (1999)
- M. Cvetic, G.W. Gibbons, D. Kubiznak, C.N. Pope, Black hole enthalpy and an entropy inequality for the thermodynamic volume. *Phys. Rev. D* **84**, 024037 (2011). [arXiv:1012.2888](https://arxiv.org/abs/1012.2888)
- B.P. Dolan, D. Kastor, D. Kubiznak, R.B. Mann, J. Traschen, Thermodynamic volumes and isoperimetric inequalities for de Sitter black holes. *Phys. Rev. D* **87**(10), 104017 (2013). [arXiv:1301.5926](https://arxiv.org/abs/1301.5926)
- D. Kubiznak, R.B. Mann, P–V criticality of charged AdS black holes. *JHEP* **1207**, 033 (2012)

36. C. Song-Bai, L. Xiao-Fang, L. Chang-Qing, *P–V* criticality of an AdS black hole in $f(R)$ gravity. *Chin. Phys. Lett.* **30**, 060401 (2013)
37. A. Belhaj, M. Chabab, H. El Moumni, M.B. Sedra, On thermodynamics of AdS black holes in arbitrary dimensions. *Chin. Phys. Lett.* **29**, 100401 (2012)
38. A. Belhaj, M. Chabab, H. El Moumni, L. Medari, M.B. Sedra, The thermodynamical behaviors of Kerr–Newman AdS black holes. *Chin. Phys. Lett.* **30**, 090402 (2013)
39. A. Belhaj, M. Chabab, H. El Moumni, K. Masmar, M.B. Sedra, Critical behaviors of 3D black holes with a scalar hair. *IJGMMP* **12**, 1550017 (2015). [arXiv:1306.2518](#) [hep-th]
40. A. Belhaj, M. Chabab, H. EL Moumni, K. Masmar, M.B. Sedra, Ehrenfest scheme of higher dimensional AdS black holes in the third-order Lovelock–Born–Infeld gravity. *Int. J. Geom. Meth. Mod. Phys.* **12**(10), 1550115 (2015). [arXiv:1405.3306](#) [hep-th]
41. A. Belhaj, M. Chabab, H. El Moumni, K. Masmar, M.B. Sedra, A. Segui, On heat properties of AdS black holes in higher dimensions. *JHEP* **1505**, 149 (2015). [arXiv:1503.07308](#) [hep-th]
42. A. Belhaj, M. Chabab, H. El Moumni, K. Masmar, M.B. Sedra, On thermodynamics of AdS black holes in M-theory. *Eur. Phys. J. C* **76**(2), 73 (2016). [arXiv:1509.02196](#) [hep-th]
43. M. Chabab, H. El Moumni, K. Masmar, On thermodynamics of charged AdS black holes in extended phases space via M2-branes background. *Eur. Phys. J. C* **76**(6), 304 (2016). [arXiv:1512.07832](#) [hep-th]
44. P. Prasia, V.C. Kuriakose, Quasinormal modes and P–V criticality for scalar perturbations in a class of dRGT massive gravity around black holes. *Gen. Rel. Grav.* **48**(7), 89 (2016). [arXiv:1606.01132](#)
45. E. Spallucci, A. Smailagic, Maxwell’s equal area law for charged Anti-de Sitter black holes. *Phys. Lett. B* **723**, 436 (2013). [arXiv:1305.3379](#)
46. J.X. Zhao, M.S. Ma, L.C. Zhang, H.H. Zhao, R. Zhao, The equal area law of asymptotically AdS black holes in extended phase space. *Astrophys. Space Sci.* **352**, 763 (2014)
47. N. Altamirano, D. Kubiznak, R.B. Mann, Z. Sherkatghanad, Thermodynamics of rotating black holes and black rings: phase transitions and thermodynamic volume. *Galaxies* **2**, 89 (2014). [arXiv:1401.2586](#)
48. S.W. Hawking, D.N. Page, Thermodynamics of black holes in Anti-de Sitter space. *Commun. Math. Phys.* **87**(4), 577 (1983)
49. A. Belhaj, M. Chabab, H. El moumni, K. Masmar, M.B. Sedra, Maxwell’s equal-area law for Gauss–Bonnet–Anti-de Sitter black holes. *Eur. Phys. J. C* **75**, 71 (2015). [arXiv:1412.2162](#)
50. C.V. Johnson, Holographic heat engines. *Class. Quant. Grav.* **31**, 205002 (2014). [arXiv:1404.5982](#)
51. E. Spallucci, A. Smailagic, Maxwell’s equal area law and the Hawking–page phase transition. *J. Grav.* **2013**, 525696 (2013). [arXiv:1310.2186](#)
52. B.P. Dolan, Vacuum energy and the latent heat of AdS–Kerr black holes. *Phys. Rev. D* **90**, 084002 (2014). [arXiv:1407.4037](#)
53. S. Janiszewski, M. Kaminski, Quasinormal modes of magnetic and electric black branes versus far from equilibrium anisotropic fluids. *Phys. Rev. D* **93**, 025006 (2016). [arXiv:1508.06993](#)
54. S. Mahapatra, Thermodynamics, phase transition and quasinormal modes with Weyl corrections. *JHEP* **1604**, 142 (2016). [arXiv:1602.03007](#)
55. J.M. Zhu, B. Wang, E. Abdalla, Object picture of quasinormal ringing on the background of small Schwarzschild Anti-de Sitter black holes. *Phys. Rev. D* **63**, 124004 (2001). [arXiv:hep-th/0101133](#)
56. B. Wang, C. Molina, E. Abdalla, Evolving of a massless scalar field in Reissner–Nordstrom Anti-de Sitter spacetimes. *Phys. Rev. D* **63**, 084001 (2001). [arXiv:hep-th/0005143](#)